Journal of Zhejiang University-SCIENCE A (Applied Physics & Engineering)
ISSN 1673-565X (Print); ISSN 1862-1775 (Online)
www.zju.edu.cn/jzus; www.springerlink.com
E-mail: jzus@zju.edu.cn

A high-dexterity low-degree-of-freedom hybrid manipulator structure for robotic lion dance*

Liang YAN†1, I-Ming CHEN†‡2, Song-huat YEO2, Yan CHEN2, Gui-lin YANG3

(1School of Automation Science and Electrical Engineering, Beihang University, Beijing 100191, China)

(2School of Mechanical and Aerospace Engineering, Nanyang Technological University, Nanyang 639798, Singapore)

(3Mechatronics Group, Singapore Institute of Manufacturing Technology, Nanyang 638075, Singapore)

†E-mail: Lyan1991@gmail.com; MIChen@ntu.edu.sg

Received Jan. 19, 2010; Revision accepted Jan. 19, 2010; Crosschecked Jan. 27, 2010

Abstract: Lion dance is a very popular and lively Chinese traditional art form. A robotic project in Singapore has been dedicated to the design and demonstration for similar traditional art forms using modern mechatronics technology. This paper deals with a novel six-degree-of-freedom (6-DOF) hybrid manipulator with high stiffness, high loading capability and high dexterity, mimicking the lion dancer's upper body motions along with the lion head movements. The design of the hybrid manipulator consists of a 2-DOF torso structure in serial configuration and a 4-DOF dual arm structure in parallel configuration. The combined 6-DOF hybrid manipulator can support the weight and dynamics of the lion head during the lion dance performance. Forward kinematics of the manipulator has been formulated and visualized for design purposes. Inverse kinematics of the hybrid manipulator were analytically derived for real-time motion control. Based on the design and modeling, a complete hybrid manipulator has been fabricated, implemented into the robotic lion, and successfully demonstrated for real robotic lion dance performance.

Key words: Parallel mechanism, Hybrid manipulator, Kinematics analysis
doi:10.1631/jzus.A1000028 **Document code:** A **CLC number:** TP24

1 Introduction

Lion dance is a traditional folk art performed in Chinese festivals, important celebrations and religious events. It is a very popular and widely seen art form in almost all Chinese communities around the world. In the lion dance, two performers dress in a lion outfit to perform coordinated acrobatic choreography that imitates lion movements (Fig. 1). The movements of the performers and the outfit, especially the lion head, are performed according to a very dynamic lion dance choreography passed down for hundreds of years. For example, the lion dance may start off from the position of a sleeping lion, then to a moving lion walking and jumping, performing acrobatics such as walking on a balance board, poles, or standing on a ball. As the dance is performed by human performers with human motion skills, it is a coordinated two-person dance form rather than a "dancing lion".

Together with Singapore Institute of Manufacturing Technology, we have designed and constructed a life-size robotic lion dance system which can perform live traditional lion dance. The aim of this project is to exploit advanced mechatronics technology to design a robotic system that can perform lion dances with the typical lion outfit, showcasing the fusion of traditional culture and robotic technology, and exploring a possible transformation into a new art form. Having recognized that the lion dance is a highly dynamic two-person performance, we first conducted field investigation and recorded complete lion dance sequences with costumes to study the basic choreography as well as its religious and cultural meanings. Secondly, we invited a lion dance troupe to perform the lion dance without the costume to capture the characteristic movements of the two performers using videos.

‡ Corresponding author

* Project supported by the collaboration between Nanyang Technological University (NTU) and Singapore Institute of Manufacturing Technology (SIMTech) under Agency for Science, Technology and Research (ASTAR)

(a) (b)

Fig. 1 Traditional lion dance in Chinese culture. (a) Lion dance; (b) Human gait

From this study, we discovered the fundamental operating principle of the lion head and its manipulation skills by the fore-performer, which is predominantly important in producing dramatic effects. Thus, in the design of the mechanical system of the robotic lion, attention was focused on duplicating the fore-performer's movements and manipulation of the lion head.

The concept of the robotic lion is illustrated in Fig. 2. In this robotic lion, a humanoid-like robot structure for the fore-performer with legs and arms is designed. A lower body structure is designed for the rear-performer for changing foot placement in the dance. The fore- and rear-performers are joined through a rigid link structure acting as the lion body. As the system is designed to focus on dance performance, two design principles are used: (1) the legs are designed to perform movements without supporting the lion's weight, so a wheeled mobile platform supports the lion body; (2) the upper body of the fore-performer, i.e., the torso and the arms, requires good dexterity and dynamic range of motions in order to perform agilely with the lion head. This study is concerned with the critical human-like fore-performer manipulation mechanism in order to produce lively lion head movements, while maintaining simple kinematic structure and fewer degrees of freedom (DOFs) than a real lion dance performer. Robotic manipulators for entertainment and performance have been previously proposed to mimic real human arm motion. A family of autonomous mobile robots named EyeBot was developed by Braunl (1999) and Braunl and Graf (1999). The arms of EyeBot are very simple with only two shoulder joints. A robot for RoboCup Humanoid League, PINO, has also been developed (Yamasaki *et al*., 2000; 2001) with shoulder and elbow joints, so that it can handle objects using multi-DOF manipulation. A similar bipedal robot, ELVIS, with human-like arm geometry has been designed (Nordin and Nordahl, 2006). A wheeled humanoid robot with 7-DOF arms has been developed (Tsay and Lai, 2006). The robot arms and head can coordinate with each other to locate and grasp the target object. The humanoid robots, WABIAN-RIV (Carbone *et al*., 2005), Sony Qrio (Sony Corporation, 2008) and Honda ASIMO (Honda Motor Corporation, 2008) all have high-DOF arms for human-robot cooperation work. Generally, the arms of these robots are open kinematic chain, and composed of serial links interconnected to each other by revolute and prismatic joints. Although open kinematic chain robot arms are relatively simple, they have insufficient mechanical stiffness, which degrades the performance of the robot under high dynamic ranges of motion. A closed kinematic chain type of mechanisms possesses the rigidity and stiffness required by the performance. A slider crank mechanism with closed kinematic chain has been proposed (Koser, 2004) for performance with a single arm structure design. This design, however, is not favorable for high payload work. A multi-input multi-output parallel-structured robot arm, robomech, is developed (Smaili and Atallah, 2005) with closed chain to perform tasks that require the simultaneous execution of coordinated multi-functions. This manipulator can only generate motions in a single plane, which apparently constrains its applications. Therefore, to provide the dexterity and stiffness required in the live performance, a novel hybrid manipulator structure is proposed for the fore-performer manipulation mechanism in the robotic lion dance system to mimic the performer's lion head manipulation movements.

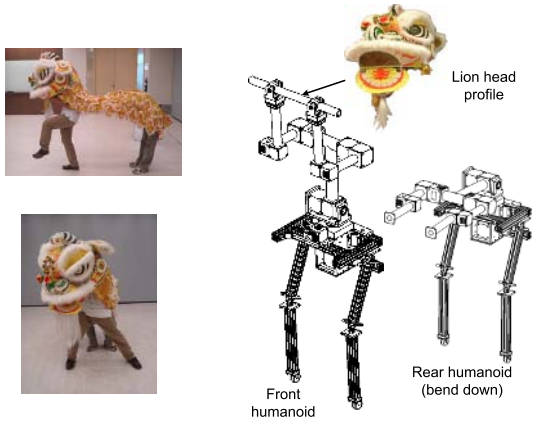

(a) (b)

Fig. 2 Humanoid structures in robotic lion dance system. (a) Lion dance; (b) Robotic lion

2 Conceptual design

2.1 Description of the 6-DOF manipulator

As illustrated in Fig. 3, the proposed 6-DOF hybrid manipulator consists of a 2-DOF serial mechanism and

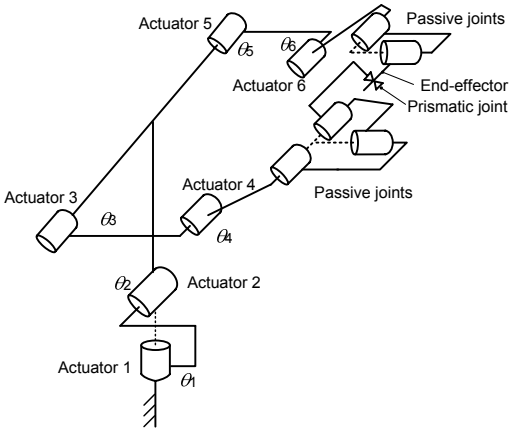

Fig. 3 Schematic drawing of the hybrid manipulator

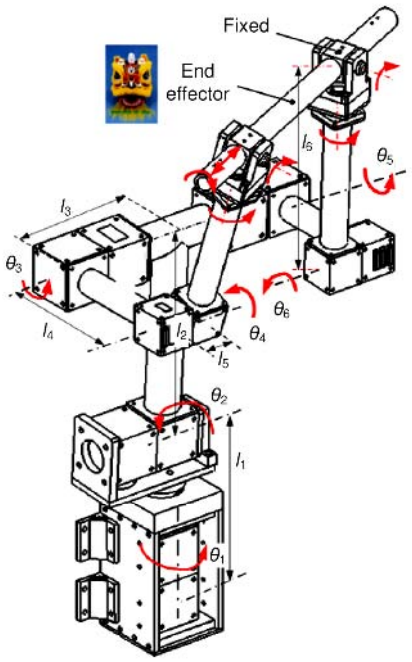

Fig. 4 Joints and dimensions of the hybrid manipulator

a 4-DOF parallel mechanism. Two actuators (actuators 1 and 2) are used to generate the rotational and tilting motions θ_1 and θ_2, respectively, for the torso joints. Actuators 3 and 4 are employed to produce the motions of shoulder joints θ_3 and θ_4, whereas actuators 5 and 6 are utilized for rotations θ_5 and θ_6. There are seven passive joint motions. The three passive rotary joints on the right arm act as a ball joint, whereas the two rotary joints on the left arm act as a universal joint. A prismatic joint lies between these two sets of rotary joints. End-effectors such as the lion head profile can be mounted on the horizontal bar which in turn is connected to the end of both arms. The two arms are assembled in a closed form, which can increase the stiffness of the structure. The external payload, the lion head, and the horizontal bar can be regarded as a single rigid body. The combined lion head and the hand bar mechanism helps to achieve high stiffness, high precision and high speed manipulation from the hybrid arms. The design of the hybrid manipulator is illustrated in Fig. 4. A horizontal bar is mounted on the arms. One end is fixed on the left arm with two-direction rotary motions, whereas the other end can produce a sliding motion relative to the right arm with rotations in three directions. In other words, the left and right arms of this manipulator are not symmetric in the structure. This closed chain structure mimics the motions of the two-arm movements of the performer manipulating the lion head for lion dance performance.

2.2 Degrees of freedom in hybrid manipulator

One important aspect of designing the robotic lion is to optimize the number of actuators (or the DOFs of the mechanism) for good performance. It is always a trade-off between the complexity of the system and capability of the system performance. Thus, determining the DOFs of the manipulation mechanism in the robotic lion is key. The number of DOFs for the hybrid mechanism can be calculated based on Kutzbach criteria as follows:

$$M = 6(N - G - 1) + \sum_{i=1}^{G} F_i, \tag{1}$$

where M is the number of DOFs of the mechanism, N is the number of bodies in the mechanism, G is the number of joints and F_i is the number of DOFs of the ith joint. For the presented parallel mechanism in the hybrid manipulator (Fig. 4), $N = 9$, $G = 9$, $F_i = 1$ for eight revolute joints, and $F_i = 2$ for one cylindrical joint. Application of Eq. (1) yields four DOFs. Together with the two DOFs of the serial mechanism in the torso, there are six DOFs in the hybrid manipulator. The number of DOFs of the hybrid manipulator determines the number of actuators used in the mechanism.

3 Analysis of forward kinematics

3.1 Link frames attachment and parameters

To describe the location of each link, a frame is attached to each link. In this study, the Denavit-Hartenberg

(D-H) convention is employed to define the links and describe the relationships between them. As indicated in Fig. 5, frames O_0 to O_8 are attached to each link, where O_0 is the base or global frame, whereas O_8 is the frame of the end-effector. From the definition, a table of link parameters can be created as shown in Table 1, where a_i is the distance along x_i from O_i to the intersection of the x_i and z_{i-1} axes; d_i is the distance along z_{i-1} from O_{i-1} to the intersection of the x_i and z_{i-1} axes; α_i is the angle between z_{i-1} and z_i measured about x_i; ϕ_i is the angle between x_{i-1} and x_i measured about z_{i-1}. ϕ_i is variable if joint i is revolute.

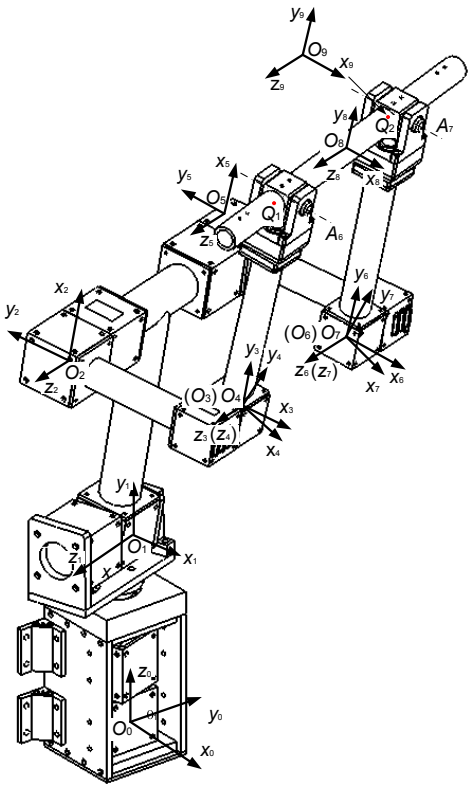

Fig. 5 Link frames on the 6-DOF hybrid manipulator

Table 1 Link parameters of 6-DOF hybrid manipulator

i	a_i	d_i	α_i	ϕ_i
1	0	l_1	90°	θ_1
2	l_2	l_3	0°	$90°+\theta_2$
3	l_4	$-l_5$	0°	$-(90°-\theta_3)$
4	0	0	0°	θ_4
5	l_2	$-l_3$	0°	$90°+\theta_2$
6	l_4	l_5	0°	$-(90°-\theta_5)$
7	0	0	0°	θ_6

3.2 Position and orientation of end-effector

3.2.1 Link transformations

The homogeneous transformation $\boldsymbol{T}_i$ of each link can be derived as follows:

$$\boldsymbol{T}_i=\begin{bmatrix}\cos\phi_i & -\sin\phi_i\cos\alpha_i & \sin\phi_i\sin\alpha_i & a_i\cos\phi_i\\ \sin\phi_i & \cos\phi_i\cos\alpha_i & -\cos\phi_i\sin\alpha_i & a_i\sin\phi_i\\ 0 & \sin\alpha_i & \cos\alpha_i & d_i\\ 0 & 0 & 0 & 1\end{bmatrix}, \tag{2}$$

where $i=1,2,...,7$. For the right arm, the transformation equation from (x_0,y_0,z_0) to (x_4,y_4,z_4) is

$$\begin{bmatrix}x_{0,Q_1}\\ y_{0,Q_1}\\ z_{0,Q_1}\\ 1\end{bmatrix}=\boldsymbol{T}_1\boldsymbol{T}_2\boldsymbol{T}_3\boldsymbol{T}_4\begin{bmatrix}0\\ l_6\\ 0\\ 1\end{bmatrix}, \tag{3}$$

where $x_{i,j}$, $y_{i,j}$ and $z_{i,j}$ indicate x, y, z coordinates of point j in the coordinate system i, respectively. Q_1 is the point on the axes intersection of the right hand and the horizontal bar. Similarly, for the left arm, the following transformation equation from (x_0,y_0,z_0) to (x_7,y_7,z_7) can be obtained:

$$\begin{bmatrix}x_{0,Q_2}\\ y_{0,Q_2}\\ z_{0,Q_2}\\ 1\end{bmatrix}=\boldsymbol{T}_1\boldsymbol{T}_5\boldsymbol{T}_6\boldsymbol{T}_7\begin{bmatrix}0\\ l_6\\ 0\\ 1\end{bmatrix}. \tag{4}$$

3.2.2 Position of end-effector

Because the three points Q_1, Q_2 and O_8 are on a line (O_8 is the point on the axis of the horizontal bar. The distance between O_8 and O_2 is l_3-l_5.), the following equations can be obtained:

$$\frac{x_{0,O_8}-x_{0,Q_2}}{x_{0,Q_1}-x_{0,Q_2}}=\frac{y_{0,O_8}-y_{0,Q_2}}{y_{0,Q_1}-y_{0,Q_2}}=\frac{z_{0,O_8}-z_{0,Q_2}}{z_{0,Q_1}-z_{0,Q_2}}=t, \tag{5}$$

$$(x_{0,O_8}-x_{0,Q_2})^2+(y_{0,O_8}-y_{0,Q_2})^2+(z_{0,O_8}-z_{0,Q_2})^2=(l_3-l_5)^2, \tag{6}$$

which results in

$$t=\frac{l_3-l_5}{\sqrt{(x_{0,Q_1}-x_{0,Q_2})^2+(y_{0,Q_1}-y_{0,Q_2})^2+(z_{0,Q_1}-z_{0,Q_2})^2}}. \tag{7}$$

Therefore, the three coordinates of point O_8 can be expressed in terms of coordinates of points Q_1 and Q_2 as

$$x_{0,O_8} = x_{0,Q_2} + (x_{0,Q_1} - x_{0,Q_2})t, \tag{8}$$

$$y_{0,O_8} = y_{0,Q_2} + (y_{0,Q_1} - y_{0,Q_2})t, \tag{9}$$

$$z_{0,O_8} = z_{0,Q_2} + (z_{0,Q_1} - z_{0,Q_2})t. \tag{10}$$

From Eqs. (3), (4), (7) and (8)–(10), the position of O_8 can be computed from the motor angles θ_1 to θ_6.

3.2.3 Orientation of end-effector

The orientation of the end-effector can be formulated from θ_1 to θ_6. The normalized direction of $\boldsymbol{y}_8$ is

$$\boldsymbol{y}_8 = \frac{\begin{bmatrix} x_{Q_2} - x_{Q_1} & y_{Q_2} - y_{Q_1} & z_{Q_2} - z_{Q_1} \end{bmatrix}^{\mathrm{T}}}{\sqrt{(x_{Q_2} - x_{Q_1})^2 + (y_{Q_2} - y_{Q_1})^2 + (z_{Q_2} - z_{Q_1})^2}}. \tag{11}$$

Similarly,

$$\boldsymbol{Q_2O_7} = \frac{\begin{bmatrix} x_{O_7} - x_{Q_2} & y_{O_7} - y_{Q_2} & z_{O_7} - z_{Q_2} \end{bmatrix}^{\mathrm{T}}}{\sqrt{(x_{O_7} - x_{Q_2})^2 + (y_{O_7} - y_{Q_2})^2 + (z_{O_7} z_{Q_2})^2}}, \tag{12}$$

where x_{O_7}, y_{O_7} and z_{O_7} can be calculated from

$$\begin{bmatrix} x_{0,O_7} \\ y_{0,O_7} \\ z_{0,O_7} \\ 1 \end{bmatrix} = \boldsymbol{T}_1\boldsymbol{T}_5\boldsymbol{T}_6\boldsymbol{T}_7 \begin{bmatrix} x_{7,O_7} \\ y_{7,O_7} \\ z_{7,O_7} \\ 1 \end{bmatrix} = \boldsymbol{T}_1\boldsymbol{T}_5\boldsymbol{T}_6\boldsymbol{T}_7 \begin{bmatrix} 0 \\ 0 \\ 0 \\ 1 \end{bmatrix}. \tag{13}$$

The direction of vector $\boldsymbol{x}_8$ can be calculated as

$$\boldsymbol{x}_8 = \boldsymbol{O_2O_7} \times \boldsymbol{y}_8. \tag{14}$$

Therefore, the orientation matrix of the end-effector is

$$\boldsymbol{R}_8 = \begin{bmatrix} \boldsymbol{x}_8 & \boldsymbol{y}_8 & \boldsymbol{x}_8 \times \boldsymbol{y}_8 \end{bmatrix} = \begin{bmatrix} r_{11} & r_{12} & r_{13} \\ r_{21} & r_{22} & r_{23} \\ r_{31} & r_{32} & r_{33} \end{bmatrix}. \tag{15}$$

On the other hand, the orientation matrix can be represented with Euler angles. Assuming that the end-effector starts with the frame coincident with the global frame, then rotates about the local z-axis by an angle of θ_z, then about the local y-axis by θ_y, finally about the local x-axis by θ_x. The general rotation matrix after these three rotations is represented as (Craig, 1989)

$$\boldsymbol{R}_8' = \begin{bmatrix} c\theta_z c\theta_y & c\theta_z s\theta_y s\theta_x - s\theta_z c\theta_x & c\theta_z s\theta_y c\theta_x + s\theta_z s\theta_x \\ s\theta_z c\theta_y & s\theta_z s\theta_y s\theta_x + c\theta_z c\theta_x & s\theta_z s\theta_y c\theta_x - c\theta_z s\theta_x \\ -s\theta_y & c\theta_y s\theta_x & c\theta_y c\theta_x \end{bmatrix}, \tag{16}$$

where $s\theta_x$, $c\theta_x$, $s\theta_y$, $c\theta_y$, $s\theta_z$, $c\theta_z$ represent $\sin\theta_x$, $\cos\theta_x$, $\sin\theta_y$, $\cos\theta_y$, $\sin\theta_z$ and $\cos\theta_z$, respectively. Comparing the elements in $\boldsymbol{R}_8$ and $\boldsymbol{R}_8'$ gives

$$\theta_y = \arcsin(-r_{31}), \theta_z = \arctan\left(\frac{r_{21}}{r_{11}}\right), \theta_x = \arctan\left(\frac{r_{32}}{r_{33}}\right).$$

Angle values between $-\pi/2$ and $\pi/2$ will be utilized.

3.3 Visualization of manipulator motions

To visualize the variation of position and orientation of the end-effector, two motor angles are selected as independent variables, whereas the rest angles are fixed at the original position.The position and orientation of point O_8 with respect to elbow joint angles, θ_4 and θ_6 are presented in Fig. 6.It can be found from Fig. 5 that when $\theta_4 = \theta_6$ and the rest motors are fixed at the initial position, O_8 is constrained on the plane of $z_0O_0x_0$. Therefore, y coordinate of O_8 in the global frame is always equal to zero. Because point Q_2 is fixed on the left hand, the movement with $\theta_4 \neq \theta_6$ pulls Q_8 to the left side of plane $z_0O_0x_0$. Therefore, y coordinate of O_8 in the global frame is always larger than zero, which is shown in Fig. 6c clearly. From Fig. 6e, the variation of z_{0,O_8} forms a taper surface, i.e., when $\theta_4 = 0$ and $\theta_6 = 0$, there is a maximum value of z_{0,O_8}. The relationship of $\theta_4 = \theta_6 = 0$ indicates that the two upper arms of the manipulator are at the upright position. Moving either elbow joint will drag O_8 down. In other words, z_{0,O_8} can achieve the highest value at the arms' upright position. The variation of θ_x, θ_y and θ_z with respect to θ_4 and θ_6 is also presented visually. It can be seen from Figs. 6b and 6f that when $\theta_4 = \theta_6$, θ_x and θ_z are always equal to zero. The orientation transformation from the coordinate system (x_0, y_0, z_0) to (x_8, y_8, z_8) can be described as three steps: one rotation about the x-axis of the moving frame is equal to zero, followed by one rotation about y-axis of the moving frame, ending with one rotation of 0° about z-axis. Particular poses of the hybrid manipulator are presented in Fig. 7. The six actuator angles along with position and orientation of the end-effector are indicated in the figure. It can be seen that the basic behavior poses useful for robotic lion dance performance can be achieved with the proposed 6-DOF hybrid manipulator.

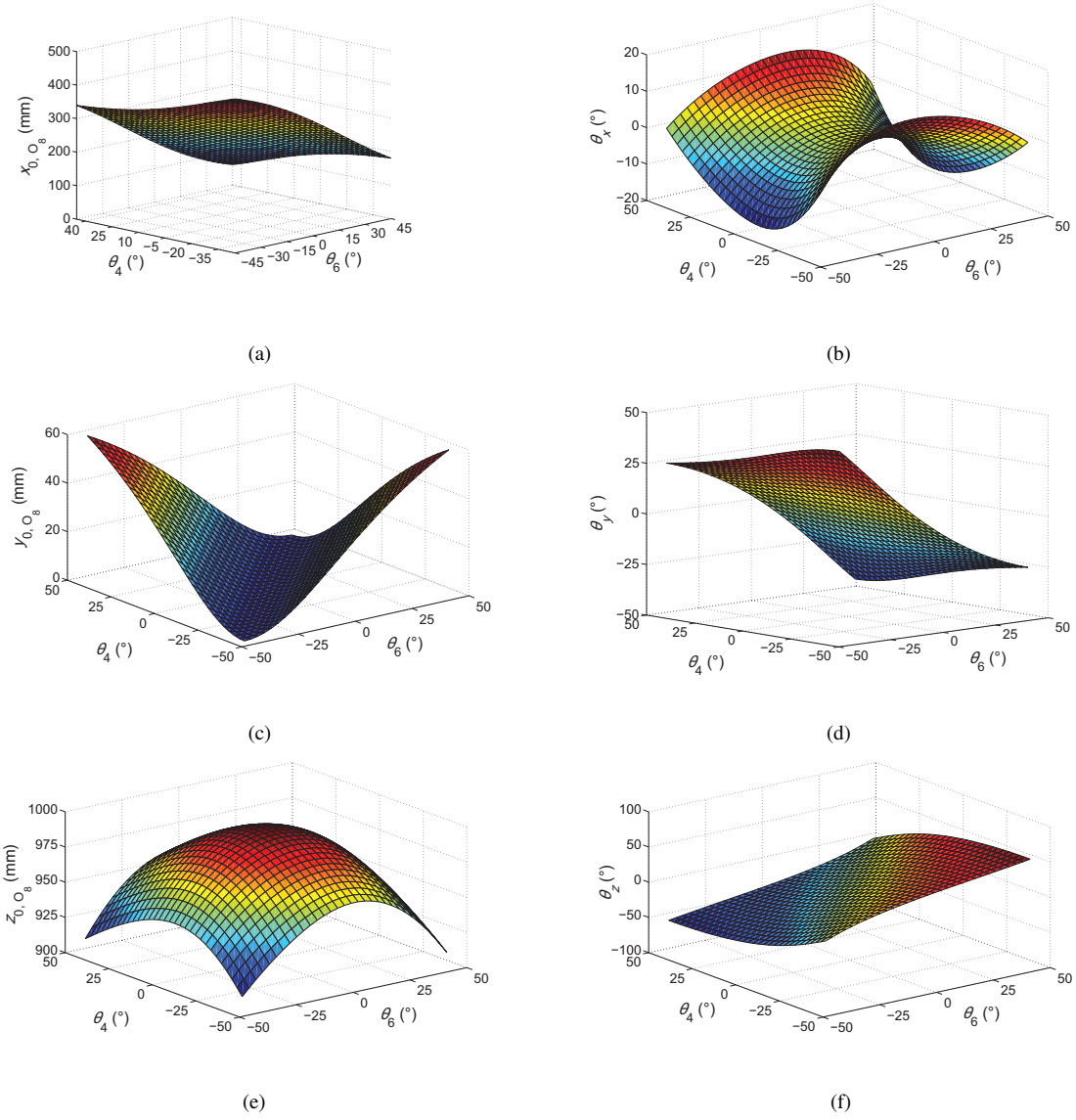

Fig. 6 Orientation and position of the end-effector vs. joint angles θ_4 and θ_6. (a) Variation of x_{0,O_8} vs. θ_4 and θ_6; (b) Variation of θ_x vs. θ_4 and θ_6; (c) Variation of y_{0,O_8} vs. θ_4 and θ_6; (d) Variation of θ_y vs. θ_4 and θ_6; (e) Variation of z_{0,O_8} vs. θ_4 and θ_6; (f) Variation of θ_z vs. θ_4 and θ_6

4 Inverse kinematics

4.1 Solution of θ_1

Point Q_2 can be calculated as ($\boldsymbol{P}_8$ stands for the position of O_8 at the end-effector in the global frame)

$$\begin{bmatrix} x_{0,Q_2} \\ y_{0,Q_2} \\ z_{0,Q_2} \\ 1 \end{bmatrix} = \begin{bmatrix} \boldsymbol{R}_8 & \boldsymbol{P}_8 \\ \boldsymbol{0} & \boldsymbol{1} \end{bmatrix} \begin{bmatrix} x_{8,Q_2} \\ y_{8,Q_2} \\ z_{8,Q_2} \\ 1 \end{bmatrix} = \begin{bmatrix} \boldsymbol{R}_8 & \boldsymbol{P}_8 \\ \boldsymbol{0} & \boldsymbol{1} \end{bmatrix} \begin{bmatrix} 0 \\ l_3 - l_5 \\ 0 \\ 1 \end{bmatrix}, \quad (17)$$

where $\boldsymbol{P}_8 = [\ x_{0,O_8} \quad y_{0,O_8} \quad z_{0,O_8}\ ]^{\mathrm{T}}$.

Imagine point Q_2 in a spherical coordinate system locating at O_0. θ_1 can be calculated directly from Q_2:

$$\theta_1 = \begin{cases} \arcsin\left(\dfrac{y_{0,Q_2}}{\sqrt{x_{0,Q_2}^2 + y_{0,Q_2}^2}}\right), & \text{for } x \geq 0, \\ -\arcsin\left(\dfrac{y_{0,Q_2}}{\sqrt{x_{0,Q_2}^2 + y_{0,Q_2}^2}}\right), & \text{for } x < 0. \end{cases} \quad (18)$$

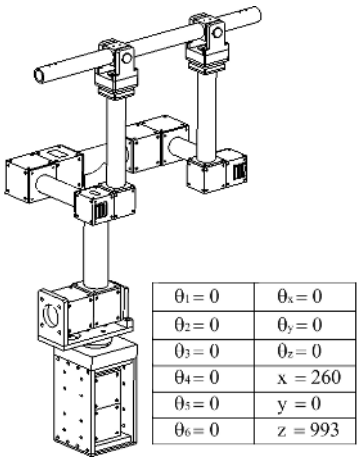

$\theta_1 = 0$	$\theta_x = 0$
$\theta_2 = 0$	$\theta_y = 0$
$\theta_3 = 0$	$\theta_z = 0$
$\theta_4 = 0$	$x = 260$
$\theta_5 = 0$	$y = 0$
$\theta_6 = 0$	$z = 993$

(a) Initial position

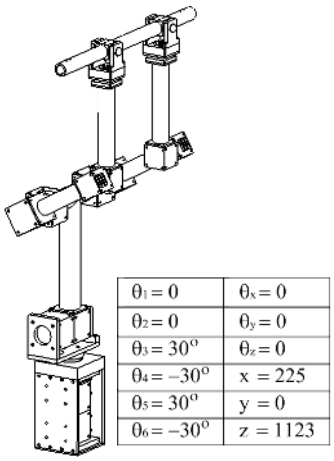

$\theta_1 = 0$	$\theta_x = 0$
$\theta_2 = 0$	$\theta_y = 0$
$\theta_3 = 30^\circ$	$\theta_z = 0$
$\theta_4 = -30^\circ$	$x = 225$
$\theta_5 = 30^\circ$	$y = 0$
$\theta_6 = -30^\circ$	$z = 1123$

(b) Raise up

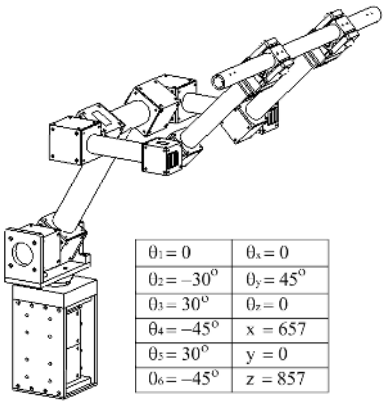

$\theta_1 = 0$	$\theta_x = 0$
$\theta_2 = -30^\circ$	$\theta_y = 45^\circ$
$\theta_3 = 30^\circ$	$\theta_z = 0$
$\theta_4 = -45^\circ$	$x = 657$
$\theta_5 = 30^\circ$	$y = 0$
$\theta_6 = -45^\circ$	$z = 857$

(c) Bend down

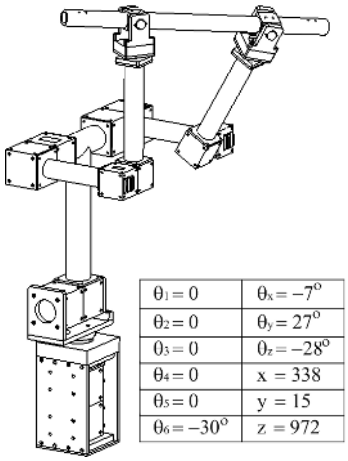

$\theta_1 = 0$	$\theta_x = -7^\circ$
$\theta_2 = 0$	$\theta_y = 27^\circ$
$\theta_3 = 0$	$\theta_z = -28^\circ$
$\theta_4 = 0$	$x = 338$
$\theta_5 = 0$	$y = 15$
$\theta_6 = -30^\circ$	$z = 972$

(d) Move left elbow

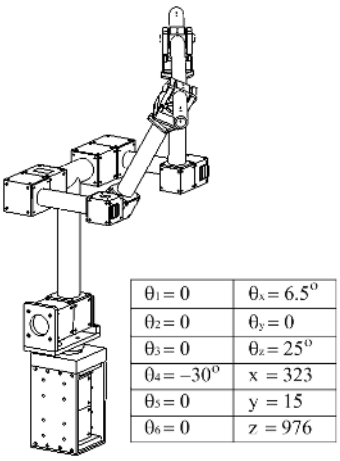

$\theta_1 = 0$	$\theta_x = 6.5^\circ$
$\theta_2 = 0$	$\theta_y = 0$
$\theta_3 = 0$	$\theta_z = 25^\circ$
$\theta_4 = -30^\circ$	$x = 323$
$\theta_5 = 0$	$y = 15$
$\theta_6 = 0$	$z = 976$

(e) Move right elbow

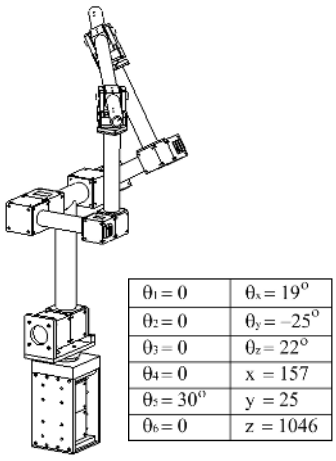

$\theta_1 = 0$	$\theta_x = 19^\circ$
$\theta_2 = 0$	$\theta_y = -25^\circ$
$\theta_3 = 0$	$\theta_z = 22^\circ$
$\theta_4 = 0$	$x = 157$
$\theta_5 = 30^\circ$	$y = 25$
$\theta_6 = 0$	$z = 1046$

(f) Move left shoulder

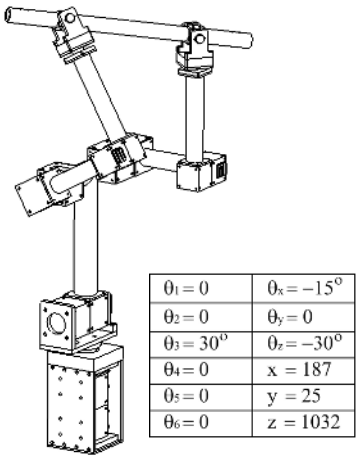

$\theta_1 = 0$	$\theta_x = -15^\circ$
$\theta_2 = 0$	$\theta_y = 0$
$\theta_3 = 30^\circ$	$\theta_z = -30^\circ$
$\theta_4 = 0$	$x = 187$
$\theta_5 = 0$	$y = 25$
$\theta_6 = 0$	$z = 1032$

(g) Move right shoulder

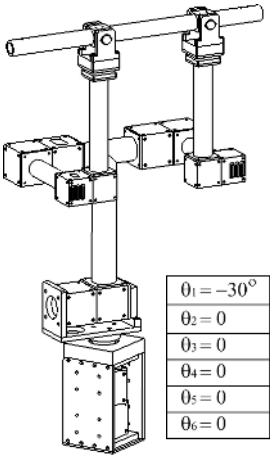

$\theta_1 = -30^\circ$	$\theta_x = 0$
$\theta_2 = 0$	$\theta_y = 0$
$\theta_3 = 0$	$\theta_z = -30^\circ$
$\theta_4 = 0$	$x = 225$
$\theta_5 = 0$	$y = -130$
$\theta_6 = 0$	$z = 993$

(h) Turn right

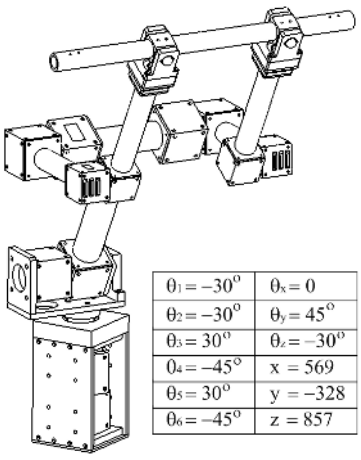

$\theta_1 = -30^\circ$	$\theta_x = 0$
$\theta_2 = -30^\circ$	$\theta_y = 45^\circ$
$\theta_3 = 30^\circ$	$\theta_z = -30^\circ$
$\theta_4 = -45^\circ$	$x = 569$
$\theta_5 = 30^\circ$	$y = -328$
$\theta_6 = -45^\circ$	$z = 857$

(i) All joints move

Fig. 7 Pose examples of the hybrid manipulator (orientation and position of end-effector vs. joint angles)

4.2 Solutions of θ_2, θ_5 and θ_6

As shown in Fig. 5, the three axes of coordinate system (x_9, y_9, z_9) are parallel to those of (x_7, y_7, z_7) respectively. It can be seen that z_7's direction can be uniquely determined by θ_1. Therefore, the direction of z_9 or z_7 in the global coordinate system is

$$\boldsymbol{z}_9 = \begin{bmatrix} \sin\theta_1 & -\cos\theta_1 & 0 \end{bmatrix}^{\mathrm{T}}. \tag{19}$$

The direction of z_8 in the global frame is

$$\boldsymbol{z}_8 = \boldsymbol{R}_8(1:3,3), \tag{20}$$

where $\boldsymbol{R}_8(1:3,3)$ is the entries at the first to third row and the third column of $\boldsymbol{R}_8$. $\boldsymbol{x}_9$ is equal to the normalization of the cross product values of $\boldsymbol{z}_8$ and $\boldsymbol{z}_9$, i.e.,

$$\boldsymbol{x}_9 = \frac{\boldsymbol{z}_8 \times \boldsymbol{z}_9}{\|\boldsymbol{z}_8 \times \boldsymbol{z}_9\|}, \tag{21}$$

where $\|\boldsymbol{z}_8 \times \boldsymbol{z}_9\|$ represents the magnitude of vector $\boldsymbol{z}_8 \times \boldsymbol{z}_9$. The orientation of (x_9, y_9, z_9) in the global frame is

$$\boldsymbol{R}_9 = \begin{bmatrix} \boldsymbol{x}_9 & \boldsymbol{z}_9 \times \boldsymbol{x}_9 & \boldsymbol{z}_9 \end{bmatrix}. \tag{22}$$

Hence, the global coordinates of point O_7 is

$$\begin{bmatrix} x_{0,O_7} \\ y_{0,O_7} \\ z_{0,O_7} \\ 1 \end{bmatrix} = \begin{bmatrix} \boldsymbol{R}_9 & \boldsymbol{P}_9 \\ \boldsymbol{0} & \boldsymbol{1} \end{bmatrix} \begin{bmatrix} x_{9,O_7} \\ y_{9,O_7} \\ z_{9,O_7} \\ 1 \end{bmatrix}, \tag{23}$$

where

$$\boldsymbol{P}_9 = \begin{bmatrix} x_{0,Q_2} & y_{0,Q_2} & z_{0,Q_2} \end{bmatrix}^{\mathrm{T}}.$$

On the other hand, the coordinates of point O_7 are

$$\begin{bmatrix} x_{0,O_7} \\ y_{0,O_7} \\ z_{0,O_7} \\ 1 \end{bmatrix} = \boldsymbol{T}_1\boldsymbol{T}_5\boldsymbol{T}_6\boldsymbol{T}_7 \begin{bmatrix} x_{7,O_7} \\ y_{7,O_7} \\ z_{7,O_7} \\ 1 \end{bmatrix} = \boldsymbol{T}_1\boldsymbol{T}_5\boldsymbol{T}_6\boldsymbol{T}_7 \begin{bmatrix} 0 \\ 0 \\ 0 \\ 1 \end{bmatrix}. \tag{24}$$

θ_2, θ_5 and θ_6 can be obtained as

$$\theta_2 = -\arcsin\left(\frac{c_x^2 + c_y^2 + l_2^2 - l_4^2}{2l_2\sqrt{c_x^2 + c_y^2}}\right) + \sigma_1, \tag{25}$$

$$\theta_5 = \arccos\left(\frac{c_x^2 + c_y^2 + l_4^2 - l_2^2}{2l_4\sqrt{c_x^2 + c_y^2}}\right) + \arcsin\left(\frac{c_x^2 + c_y^2 + l_2^2 - l_4^2}{(2l_2\sqrt{c_x^2 + c_y^2})}\right), \tag{26}$$

$$\theta_6 = \arcsin((l_4\cos(\theta_2+\theta_5) - l_2\sin\theta_2 - c_{x,2})/l_6) - (\theta_2 + \theta_5), \tag{27}$$

where $\dfrac{c_y}{\sqrt{c_x^2 + c_y^2}} = \sin\sigma_1$, $\dfrac{c_x}{\sqrt{c_x^2 + c_y^2}} = \cos\sigma_1$, and

$$\begin{bmatrix} c_x \\ c_y \\ c_z \\ 1 \end{bmatrix} = \begin{bmatrix} x_{0,O_7}\cos\theta_1 + y_{0,O_7}\sin\theta_1 \\ z_{0,O_7} - l_1 \\ x_{0,O_7}\sin\theta_1 - y_{0,O_7}\cos\theta_1 \\ 1 \end{bmatrix}, \tag{28}$$

$$c_{x,2} = x_{0,O_2}\cos\theta_1 + y_{0,O_2}\sin\theta_1. \tag{29}$$

4.3 Solution of θ_3 and θ_4

When the position of point Q_2 and the orientation of the end-effector are determined, the intersection of the horizontal bar axis and the plane of $x_4O_4y_4$, point Q_1, is uniquely fixed. From point Q_1, θ_3 and θ_4 can thus be solved. The plane of $x_4O_4y_4$ can be represented in the global coordinate system as

$$\frac{x_0\sin\theta_1}{l_3} + \frac{y_0\cos\theta_1}{l_3} = 1. \tag{30}$$

The axis of the horizontal bar can be represented with

$$\frac{x_0 - x_{0,Q_2}}{x_{0,O_8} - x_{0,Q_2}} = \frac{y_0 - y_{0,Q_2}}{y_{0,O_8} - y_{0,Q_2}} = \frac{z_0 - z_{0,Q_2}}{z_{0,O_8} - z_{0,Q_2}} = t. \tag{31}$$

Substituting Eq. (31) into Eq. (30) gives

$$t = \frac{l_3 - x_{0,Q_2}\sin\theta_1 - y_{0,Q_2}\cos\theta_1}{(x_{0,O_8} - x_{0,Q_2})\sin\theta_1 + (y_{0,O_8} - y_{0,Q_2})\cos\theta_1}. \tag{32}$$

Therefore, the values of x_{0,Q_1}, y_{0,Q_1} and z_{0,Q_1} are

$$\begin{aligned} x_{0,Q_1} &= x_{0,Q_2} + t(x_{0,O_8} - x_{0,Q_2}), \\ y_{0,Q_1} &= y_{0,Q_2} + t(y_{0,O_8} - y_{0,Q_2}), \\ z_{0,Q_1} &= z_{0,Q_2} + t(z_{0,O_8} - z_{0,Q_2}). \end{aligned} \tag{33}$$

The transformation for the right arm in Eq. (3) leads to

$$\begin{bmatrix} -\sin(\theta_2+\theta_3+\theta_4)l_6 + l_4\cos(\theta_2+\theta_3) - l_2\sin\theta_2 \\ \cos(\theta_2+\theta_3+\theta_4)l_6 + l_4\sin(\theta_2+\theta_3) + l_2\cos\theta_2 \\ -l_5 + l_3 \\ 1 \end{bmatrix} = \begin{bmatrix} c_{x,3} \\ c_{y,3} \\ c_{z,3} \\ 1 \end{bmatrix},$$

where

$$\begin{bmatrix} c_{x,3} \\ c_{y,3} \\ c_{z,3} \\ 1 \end{bmatrix} = \begin{bmatrix} x_{0,Q_1}\cos\theta_1 + y_{0,Q_1}\sin\theta_1 \\ z_{0,Q_1} - l_1 \\ x_{0,Q_1}\sin\theta_1 - y_{0,Q_1}\cos\theta_1 \\ 1 \end{bmatrix}. \tag{34}$$

From Eq. (34), the following equation is obtained

$$(c_{x,3}+l_2\sin\theta_2)\cos(\theta_2+\theta_3)+(c_{y,3}-l_2\cos\theta_2)\sin(\theta_2+\theta_3)=\frac{-l_6^2+(c_{x,3}+l_2\sin\theta_2)^2+(c_{y,3}-l_2\cos\theta_2)^2+l_4^2}{2l_4}. \quad (35)$$

Let $\sin\sigma_2=\dfrac{c_{x,3}+l_2\sin\theta_2}{\sqrt{(c_{x,3}+l_2\sin\theta_2)^2+(c_{y,3}-l_2\cos\theta_2)^2}}$ and $\cos\sigma_2=\dfrac{c_{y,3}-l_2\cos\theta_2}{\sqrt{(c_{x,3}+l_2\sin\theta_2)^2+(c_{y,3}-l_2\cos\theta_2)^2}}$.

Eq. (35) can be reorganized, and thus the following result can be obtained

$$\theta_3=\arcsin\left[\frac{-l_6^2+(c_{x,3}+l_2\sin\theta_2)^2+(c_{y,3}-l_2\cos\theta_2)^2+l_4^2}{2l_4\sqrt{(c_{x,3}+l_2\sin\theta_2)^2+(c_{y,3}-l_2\cos\theta_2)^2}}\right]-(\theta_2+\sigma_2). \quad (36)$$

Similarly, θ_4 can be calculated from Eq. (34)

$$\theta_4=\arcsin\left[\frac{-c_{x,3}+l_4\cos(\theta_2+\theta_3)-l_2\sin\theta_2}{l_6}\right]-(\theta_2+\theta_3). \quad (37)$$

From Eqs. (18), (**??**), (**??**), (27), (36) and (37), the values of six joint angles are solved.

5 System development

The 6-DOF hybrid manipulator has been developed as shown in Fig. 8. Intelligent self-contained motors from PowerCube are selected as the actuating elements of the robotic lion dance system due to its ease of programming, installation, and modularity in design. Six PowerCube servo motors with high precision harmonic drive gear box are mounted on the torso joints, shoulder joints as well as elbow joints. PowerCube PR 090 with high torque output (nominal torque 72 N·m) is used for the torso joints, and PowerCube PR 070 with relatively low torque output (nominal torque 23 N·m) is used for the rest joints. The end-effector, such as the lion head, can be mounted on top of the manipulator. By actuating the motors, 6-DOF motions of the end-effector can be generated. The hybrid manipulator with the assembled lion head is shown in Fig. 9a. A mechanism with two linear actuators is designed inside the lion head to control the opening and closing of the mouth and eyes. Fig. 9b presents the fully assembled body of the robotic lion dance system. The hybrid manipulator is placed inside the lion profile to create head motions. The movement of the lion head is demonstrated in Fig. 10.

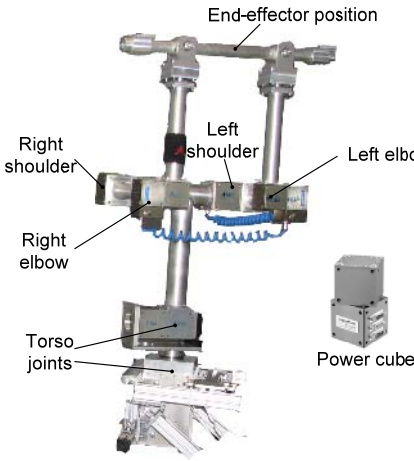

Fig. 8 Research prototype of the hybrid manipulator

(a) Assembled lion head (b) Robotic lion

Fig. 9 Hybrid manipulator in robotic lion dance system

6 Conclusion

In this work, a hybrid manipulator with torso and arm movements is proposed for a life-size robotic lion dance system to achieve dexterous movement with 6-DOFs in the lion head, including three translational and three rotational motions. The robotic arms are designed with closed kinematic chains to increase stiffness and load capability while providing highly dexterous movements. The forward and inverse kinematics have been formulated analytically. Solutions to the kinematics benefit the real-time motion control and design of the manipulator. Hardware for the hybrid manipulator has been designed and fabricated, as well as implemented in the life-size interactive robotic lion dance system. The completed robotic lion dance system has been successfully demonstrated at the opening ceremony of Fushionopolis, the most important R&D com-

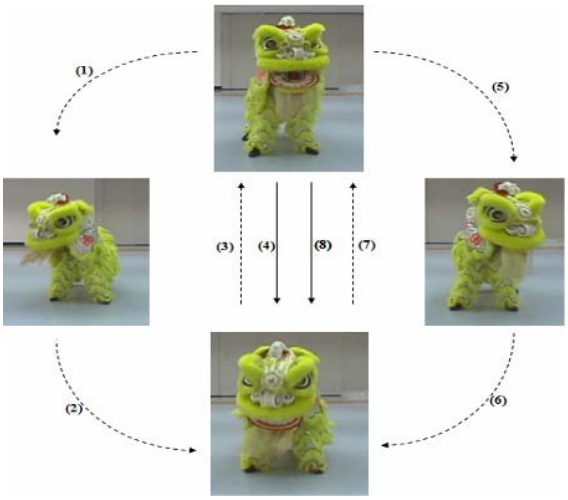

(a) Human dance

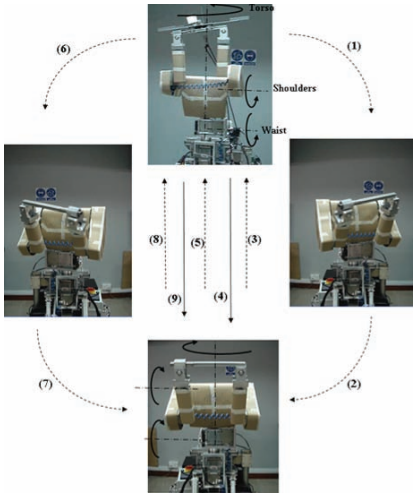

(b) Robot dance

Fig. 10 Bowling motion by moving head in a circular path

plex in Singapore. The live performance of the robotic lion dance system can be seen on Youtube (http://www.youtube.com/watch?v=dleuPL_PW8E). Further research will be carried out to integrate the fore- and rear-performers as an organic whole, and thus to achieve more complex motions similar to that of human performers.

Acknowledgement

The authors would like to acknowledge the efforts from Singapore Institute of Manufacturing Technology (SIMTech) project leaders Jenny ANG, Boon Siew HAN, Desmond HO. The efforts of Nanyang Technological University (NTU) team from S. H. TEE, A. FOONG, K. WONG, C. H. NG, C. W. NG, Y. X. TAN, T. A. N. NGUYEN, W. L. TAN, W. H. CHAI, and S. Y. LIU are also acknowledged.

References

Braunl, T., 1999. Eyebot: A Family of Autonomous Mobile Robots. Proceeding of 6th International Conference on Neural, p.645-649.

Braunl, T., Graf, B., 1999. Autonomous Mobile Robots with Onboard Vision and Local Intelligence. Proceeding of 2nd IEEE Workshop on Perception for Mobile Agents, p.51-57.

Carbone, G., Lim, H., Takanishi, A., Ceccarelli, M., 2005. Stiffness analysis of biped humanoid robot wabian-riv. *Mechanism and Machine Theory*, **41**:17-40. [doi:10.1016/j.mechmachtheory.2005.05.001]

Craig, J., 1989. Introduction to Robotics: Mechanics and Control. Addison- Wesley Publishing Company, USA.

Honda Motor Corporation, 2008. Humanoid robot ASIMO. Available from http://world.honda.com/ASIMO/ [Accessed on July 30, 2008].

Koser, K., 2004. A slider crank mechanism based robot arm performance and dynamic analysis. *Mechanism and Machine Theory*, **39**:169-182. [doi:10.1016/S0094-114X(03)00112-5]

Nordin, P., Nordahl, M., 2006. An Evolutionary Architecture for a Humanoid Robot. Conference on the Automatic Evolution of Computer Programs and Its Applications, p.57-62.

Smaili, A., Atallah, N., 2005. A three-dof robomech: Architecture, optimum synthesis and introduction to compliant robomechs. *Mechanism and Machine Theory*, **40**:1195-1206. [doi:10.1016/j.mechmachtheory.2004.11.005]

Sony Corporation, 2008. Humanoid robot SDR-4X II. Available from http://www.sony.net/SonyInfo/News/Press/200303/03-0324E/ [Accessed on July 30, 2008].

Tsay, T., Lai, H., 2006. Design and Control of a Humanoid robot. Proceedings of the 2006 IEEE/RSJ International Conference on Intelligent Robots and Systems, p.2002-2007.

Yamasaki, F., Matsui, T., Miyashita, T., Kitano, H., 2000. Pino the Humanoid: A basic Architecture. Proceeding of the Fourth International Workshop on RoboCup, p.167-176.

Yamasaki, F., Matsui, T., Miyashita, T., Kitano, H., 2001. Pino the Humanoid that Walk. Proceeding of the First IEEE-RAS International Conference on Humanoid Robots, p.34-47.